

Numerical evidence for the spin-Peierls state in the frustrated quantum antiferromagnet

P. W. Leung and Ngar-wing Lam

Physics Department, Hong Kong University of Science and Technology, Clear Water Bay, Hong Kong

(May 13, 2018)

Abstract

We study the spin- $\frac{1}{2}$ Heisenberg antiferromagnet with an antiferromagnetic J_3 (third nearest neighbor) interaction on a square lattice. We numerically diagonalize this “ J_1 - J_3 ” model on clusters up to 32-sites and search for novel ground state properties as the frustration parameter J_3/J_1 changes. For “larger” J_3/J_1 we find enhancement of incommensurate spin order, in agreement with spin-wave, large- N expansions, and other predictions. But for intermediate J_3/J_1 , the low lying excitation energy spectrum suggests that this incommensurate order is short-range. In the same region, the first excited state has the symmetries of the columnar dimer (spin-Peierls) state. The columnar dimer order parameter suggests the presence of long-range columnar dimer order. Hence, this spin-Peierls state is the best candidate for the ground state of the J_1 - J_3 model in an intermediate J_3/J_1 region.

The phase diagram of the frustrated spin- $\frac{1}{2}$ Heisenberg antiferromagnet has received much interest in recent years. On a square lattice, frustration can be introduced by further-than-nearest neighbor antiferromagnetic couplings. Short-range interactions up to a distance of two lattice constants have been studied. This is the “ J_1 - J_2 - J_3 ” model, which is described by the Hamiltonian

$$\mathcal{H} = J_1 \sum_{nn} \mathbf{S}_i \cdot \mathbf{S}_j + J_2 \sum_{2nn} \mathbf{S}_i \cdot \mathbf{S}_j + J_3 \sum_{3nn} \mathbf{S}_i \cdot \mathbf{S}_j, \quad (1)$$

where the sums run over all first, second, and third nearest neighbors, and all $J_i > 0$. The classical phase diagram of this model is well-known to have transition lines between Néel, collinear, and spiral states [1]. The critical line separating the Néel and spiral states, $J_1 - 2J_2 - 4J_3 = 0$, is called the classical critical line (CCL). The quantum phase diagram is less clear. When the frustration is small (at small J_2 and J_3), the model possesses Néel order. Various analytical studies including linear spin-wave [2,3] and mean-field theories [5] have shown that the ground state possesses collinear and spiral (incommensurate) spin order at large J_2 and J_3 respectively. The ground state at intermediate J_2 and J_3 , particularly along the quantum analog of the CCL, is still controversial. While some theories [2–4] predict that frustration and quantum fluctuation destroy the Néel order to form a state without spin order, others [5,6] predict that quantum fluctuation can stabilize the Néel state along this critical line. Nevertheless, it seems likely that in between the Néel and spiral phases, there exists an intermediate state without spin order. Large- N expansions of the unfrustrated antiferromagnet [7] predict that this intermediate state is spontaneously dimerized. This is supported by series expansion on the J_1 - J_2 - J_3 model [1], although the former (Ref. [7]) did not treat the frustration due to J_2 and J_3 explicitly. On the other hand, spin-wave theory [2,3,6] predicts that this intermediate state is a spin-liquid.

The search for a spin-liquid state in low-dimensional quantum antiferromagnets has long been a fascinating problem. Such a state is most likely to be found in frustrated systems with large quantum fluctuations. Therefore, the region along the quantum analog of the CCL in the J_1 - J_2 - J_3 model is a good place to search for a spin-liquid state, although other

kinds of long-range order (such as spin-Peierls order) have been proposed in the same region. Since the location of this critical line is unknown, it is tedious to work with two adjustable parameters J_2 and J_3 . Most numerical diagonalization studies of the frustrated Heisenberg model have been for $J_3 = 0$ [8,9]. A recent study [6] has suggested that the end of the critical line on the J_2 axis is a Lifshitz point and thus not representative of the whole critical line. The purpose of this letter is to study this model on the J_3 axis. In the following, we will take $J_1 = 1$ and $J_2 = 0$.

Using the Lanczos algorithm, we are able to diagonalize this J_1 - J_3 model on a 32-site square cluster. Most results in this letter are obtained from the 16-site (4×4) and 32-site square lattices. It is obvious that the 16-site lattice is too small to include the J_3 interaction because each site has only two (instead of four) distinct third nearest neighbors. Hence we will use results obtained from the 16-site system for comparison only. Finite-size scaling of the 16- and 32-site results will not be reliable, except perhaps at small J_3 .

It is well known that for $J_3 = 0$, the ground state of the J_1 - J_3 model exhibits long-range Néel order [10]. Fig. 1 shows the finite-size plot of the staggered magnetization m^\dagger , defined as $m^{\dagger 2} = S(\pi, \pi)/N$ (see Eq. 2). The system sizes are $N = 16, 24$ [11], and 32. The $1/\sqrt{N}$ dependence is taken from spin-wave theory for the unfrustrated case [12]. We can see that at $J_3 = 0.3$, m^\dagger extrapolates to a finite value as $N \rightarrow \infty$. But the linear extrapolation fails at $J_3 = 0.35$. Hence we conclude that the Néel order persists at least up to $J_3 = 0.3$ in the thermodynamic limit. To study the spin order as J_3 increases further, we calculate the static structure factor,

$$S(\mathbf{q}) = \frac{1}{N} \sum_{kl} e^{i\mathbf{q} \cdot (\mathbf{R}_k - \mathbf{R}_l)} \langle \mathbf{S}_k \cdot \mathbf{S}_l \rangle. \quad (2)$$

Fig. 2 shows $S(\mathbf{q})$ for the 32-site square lattice at different J_3 . It clearly shows that as J_3 increases from zero, the peak shifts from (π, π) to $(\frac{3\pi}{4}, \frac{3\pi}{4})$ at $J_3 \sim 0.5$, and then to $(\frac{\pi}{2}, \frac{\pi}{2})$ at $J_3 \sim 0.7$. This shows that the Néel order vanishes as J_3 increases and another spin order develops which has ordering vector along the $(1, 1)$ direction. If the system possesses incommensurate spin order, the peak in $S(\mathbf{q})$ should shift continuously from (π, π) to $(\frac{\pi}{2}, \frac{\pi}{2})$

as J_3 increases. Due to the discrete nature of the cluster, such a continuous shift along the $(1, 1)$ direction is not possible. Nevertheless, Fig. 2 does indicate that incommensurate spin order develops as J_3 increases. We also calculate the dynamic structure factor [8], $S(\mathbf{q}, \omega)$. Sharp low energy peaks are found at momenta along the $(1, 1)$ direction. As J_3 increases, the lowest energy peak changes from (π, π) to $(\frac{3\pi}{4}, \frac{3\pi}{4})$ at $J_3 \sim 0.5$, and then to $(\frac{\pi}{2}, \frac{\pi}{2})$ at $J_3 \sim 0.7$, indicating that the Néel order vanishes and the system develops another spin order which has ordering vector along the $(1, 1)$ direction.

To study whether this incommensurate spin order is long-range, we calculate the twist correlation function [13],

$$\chi_t = \left\langle \left| \frac{1}{N} \sum_{\mathbf{r}} \mathbf{S}_{\mathbf{r}} \times (\mathbf{S}_{\mathbf{r}+\mathbf{x}} + \mathbf{S}_{\mathbf{r}+\mathbf{y}}) \right|^2 \right\rangle, \quad (3)$$

where \mathbf{x} and \mathbf{y} are unit vectors. We expect χ_t to be independent of N for large enough N if the system possesses long-range incommensurate spin order. Fig. 3(a) shows χ_t in the 16- and 32-site systems at different J_3 . In both systems, χ_t is enhanced at J_3 larger than about 0.4. This enhancement suggests the existence of incommensurate spin order at large J_3 , which is consistent with the findings from the static and dynamic structure factors discussed above. However, only spin-wave excitations will show up as peaks in $S(\mathbf{q}, \omega)$. Therefore, it does not exclude the existence of singlet excitations, especially at intermediate J_3 . In particular it is difficult to judge from Fig. 3(a) whether the incommensurate order is long-range at intermediate J_3 .

If a system possesses a broken symmetry in the thermodynamic limit, the ground state of the finite system will still be fully symmetric. In this case the ground state expectation of the appropriate order parameter will have long-range correlations, and there will exist low lying excited states with the appropriate symmetries whose energy gaps vanish in the thermodynamic limit [14]. Consequently, we can use the low lying energy levels of a finite system to study the possible existence of long-range order. Fig. 4 shows the energies of a few low lying eigenstates in the 32-site system. For J_3 smaller than about 0.4, the first excited state is a triplet with momentum (π, π) , consistent with the existence of Néel order

for small J_3 . We denote this state as E_{T1} . For J_3 larger than about 0.85, the first excited state is a triplet with momentum $(\frac{\pi}{2}, \frac{\pi}{2})$. We denote this state as E_{T2} . E_{T1} and E_{T2} are the two spin-wave excitations which show up as low energy peaks in $S(\mathbf{q}, \omega)$. However, at intermediate J_3 , states with momentum $(\frac{3\pi}{4}, \frac{3\pi}{4})$ are never the first excited state. We denote the first excited state in this region as E_S . It is a two-fold degenerate singlet pair, one with momentum $(0, \pi)$ and the other with $(\pi, 0)$. Both are odd under reflection along the direction orthogonal to their momenta. The symmetries of the E_S state resemble the columnar dimer state [15]. In this state, nearest neighbor spin pairs form singlets (dimers), and these dimers freeze into a columnar order. It is four-fold degenerate, and can form four states with distinct symmetries: two with zero momentum, of which one is fully symmetric while the other is odd under rotation; and two with momenta $(0, \pi)$ and $(\pi, 0)$. The last two have the same symmetries as the degenerate E_S state.

Since the finite system always has a first excited state no matter whether the ground state possesses true long-range order, the results of the above study of the low lying states alone are not sufficient to show the existence of dimer order. The next evidence comes from the order parameter for the columnar dimer state [16],

$$\theta_{\mathbf{r}}^{dim} = (-1)^{r_x} \mathbf{S}_{\mathbf{r}} \cdot \mathbf{S}_{\mathbf{r}+\mathbf{x}} + i(-1)^{r_y} \mathbf{S}_{\mathbf{r}} \cdot \mathbf{S}_{\mathbf{r}+\mathbf{y}}. \quad (4)$$

In finite-size calculations, we examine the correlation function

$$\chi_{dim} = \left\langle \left| \frac{1}{N} \sum_{\mathbf{r}} \theta_{\mathbf{r}}^{dim} \right|^2 \right\rangle. \quad (5)$$

If the ground state has long-range columnar dimer order, $\chi_{dim} \sim O(1)$. Fig. 3(b) shows χ_{dim} at various J_3 in the 16- and 32-site systems. Both systems have a peak in χ_{dim} , indicating that columnar dimer order is enhanced in the corresponding region of J_3 . In the 32-site system, the peak is at $J_3 \sim 0.7$, which corresponds to the minimum energy gap between E_0 and E_S in Fig. 4. The different peak positions in Fig. 3(b) may be due to finite-size effect of the 16-site lattice as discussed above. This effect also prevents us from doing a reliable finite-size scaling study of the peak values of χ_{dim} .

The dimer correlations can be demonstrated clearly by calculating the dimer-dimer correlation function [17] defined as

$$C_{(i,j)(k,l)} = \langle (\mathbf{S}_i \cdot \mathbf{S}_j)(\mathbf{S}_k \cdot \mathbf{S}_l) \rangle - \langle \mathbf{S}_i \cdot \mathbf{S}_j \rangle^2, \quad (6)$$

where the bracket (m, n) denotes nearest neighbor sites. A dimer liquid state will display short-range structure in $C_{(i,j)(k,l)}$ but decrease to zero at large dimer separations. On the other hand, a dimer solid, or spin-Peierls state, will continue to show periodic oscillations reflecting the underlying long-range order. $C_{(i,j)(k,l)}$ for all inequivalent dimer pairs of the 32-site lattice evaluated at $J_3 = 0.7$ are tabulated in Table I. Fig. 5 is a pictorial representation of $C_{(i,j)(k,l)}$. The reference bond (i, j) is represented by a double line. For all other bonds (k, l) , the magnitude of $C_{(i,j)(k,l)}$ is represented by the thickness of the line joining sites k and l . Solid lines represent positive correlation, and broken lines represent negative or anti-correlation. It is clear that nearest neighbor spin pairs tend to form dimers, and the dimers are arranged in a columnar fashion. The dimer-dimer correlations do not decrease appreciably in the largest dimer separation allowed in our system size.

To conclude, our numerical results show that Néel order in the J_1 - J_3 model is stable up to $J_3 > 0.3$, as compared to $J_3 = 0.25$ in the classical case. This could be the result of the CCL being moved to much larger J_2 and J_3 values by quantum fluctuation [6], when the Néel state is stabilized (order from disorder) and the spiral state is destabilized along the critical line. Our results further show that the model is likely to have a spin-Peierls state between the Néel state (at small J_3) and the incommensurate state (at large J_3), in agreement with theoretical predictions [1,7,18]. In particular, Ref. [7] predicted that the dimerized patterns depend on the spin S , and our results agree with it for $S = 1/2$. We would like to remark that Ref. [7] did not treat the frustration explicitly, and it is not trivial that it gives the right prediction along the quantum analog of the CCL. But when the same analysis is extended to include frustrations due to J_2 and J_3 , similar dimerization patterns are found [19]. At large J_3 , we believe, as our results show, that the model possesses incommensurate spin order. But our finite cluster has no wave vector from $(\frac{3\pi}{4}, \frac{3\pi}{4})$ to $(\frac{\pi}{2}, \frac{\pi}{2})$ along the $(1, 1)$ direction.

Hence we are not able to locate the transition point to the incommensurate state nor to study the order of the transition.

We thank T. K. Ng and R. J. Gooding for very useful discussions. NWL acknowledges support from T.K. Ng and K. Y. Szeto through the Hong Kong Research Grant Council (RGC) contract number UST123/92E. Part of the numerical diagonalizations were performed on an HP workstation cluster at the Center for Computing and Communication Services (CCST) of the Hong Kong University of Science and Technology. Technical support provided by the CCST staff is gratefully acknowledged.

REFERENCES

- [1] M. P. Gelfand, R. R. P. Singh, and D. A. Huse, Phys. Rev. B **40**, 10801 (1989).
- [2] P. Chandra and B. Doucot, Phys. Rev. B **38**, 9335 (1988); P. Locher, *ibid* **41**, 2537 (1990); A. V. Chubukov, *ibid* **44**, 392 (1991).
- [3] A. Moreo, E. Dagotto, Th. Jolicoeur, and J. Riera, Phys. Rev. B **42**, 6283 (1990);
- [4] L. B. Ioffe and A. I. Larkin, Int. J. Mod. Phys. B **2**, 203 (1988).
- [5] S. Sachdev and N. Read, Phys. Rev. Lett. **66**, 1773 (1991). For a review of this result see S. Sachdev, *unpublished*.
- [6] J. Ferrer, Phys. Rev. B **47**, 8769 (1993).
- [7] N. Read and S. Sachdev, Phys. Rev. Lett. **62**, 1694 (1989).
- [8] D. Poilblanc, E. Gagliano, S. Bacci, and E. Dagotto, Phys. Rev. B **43**, 10970 (1991).
- [9] E. Dagotto and A. Moreo, Phys. Rev. Lett. **63**, 2148 (1989); F. Figueirido, A. Karlhede, S. Kivelson, S. Sondhi, M. Rocek, and D. S. Rokhsar, Phys. Rev. B **41**, 4619 (1990); H. J. Schulz and T. A. L. Ziman, Europhys. Lett. **18**, 355 (1992); H. J. Schulz, T. A. L. Ziman, and D. Poilblanc, (unpublished). See also Ref. [3].
- [10] E. Manousakis, Rev. Mod. Phys. **63**, 1 (1991), and references therein.
- [11] This 24-site rectangular cluster was first introduced in R. J. Gooding, K. J. E. Vos, and P. W. Leung, Phys. Rev. B **49**, 4119 (1994). Although it does not have square symmetry, it has many allowed wave vectors along the (1, 1) direction which make it suitable for studying incommensurate spin order.
- [12] H. Neuberger and T. A. L. Ziman, Phys. Rev. B **39**, 2608 (1989).
- [13] P. Chandra, P. Coleman, and A. I. Larkin, Phys. Rev. Lett. **64**, 88 (1990).
- [14] P. Horsch and W. Von der Linden, Z. Phys. B **72**, 181 (1988).

- [15] D. Rokhsar and S. Kivelson, Phys. Rev. Lett. **61**, 2376 (1988).
- [16] S. Sachdev, Phys. Rev. B **40**, 5204 (1989).
- [17] P. W. Leung and V. Elser, Phys. Rev. B **47**, 5459 (1993).
- [18] S. Sachdev and R. N. Bhatt, Phys. Rev. B **41**, 9323 (1990).
- [19] T. K. Ng, private communication.

FIGURES

FIG. 1. Finite-size plot of the staggered magnetization m^\dagger at different J_3 . The straight lines are the best fit to the data. The dotted lines are straight lines joining the data points.

FIG. 2. The static structure factor for the 32-site lattice at different values of J_3 .

FIG. 3. (a) χ_t and (b) χ_{dim} at different J_3 in the 16-site (\bullet) and 32-site ($+$) systems.

FIG. 4. Lowest energy states in different momentum sectors at different J_3 in the 32-site system. E_0 is the ground state. E_{T1} and E_{T2} are spin triplets while E_S is a spin singlet. For the purpose of clarity, lowest energy states in other momentum sectors and the second lowest energy state with momentum $\mathbf{q} = (0, 0)$ are not shown. These states have higher energy than the second lowest energy states shown in the figure.

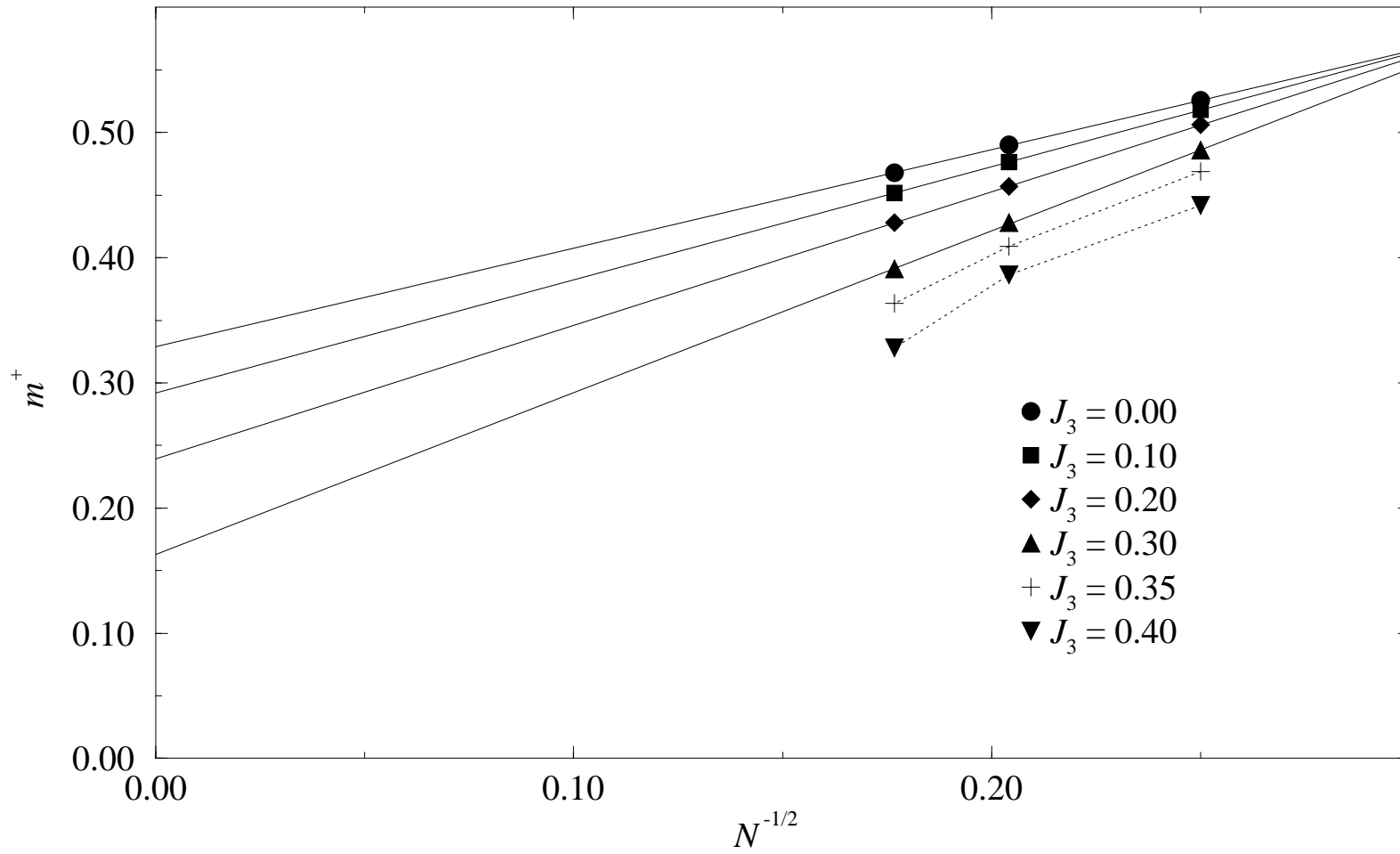
FIG. 5. Dimer-dimer correlation function $C_{(19,23)(k,l)}$ of the 32-site system at $J_3 = 0.7$. The reference bond (19, 23) is represented by a double line. The magnitude of $C_{(19,23)(k,l)}$ is proportional to the thickness of the line joining the pair of sites (k, l) . The solid line means $C_{(19,23)(k,l)}$ is positive, and the broken line means $C_{(19,23)(k,l)}$ is negative.

TABLES

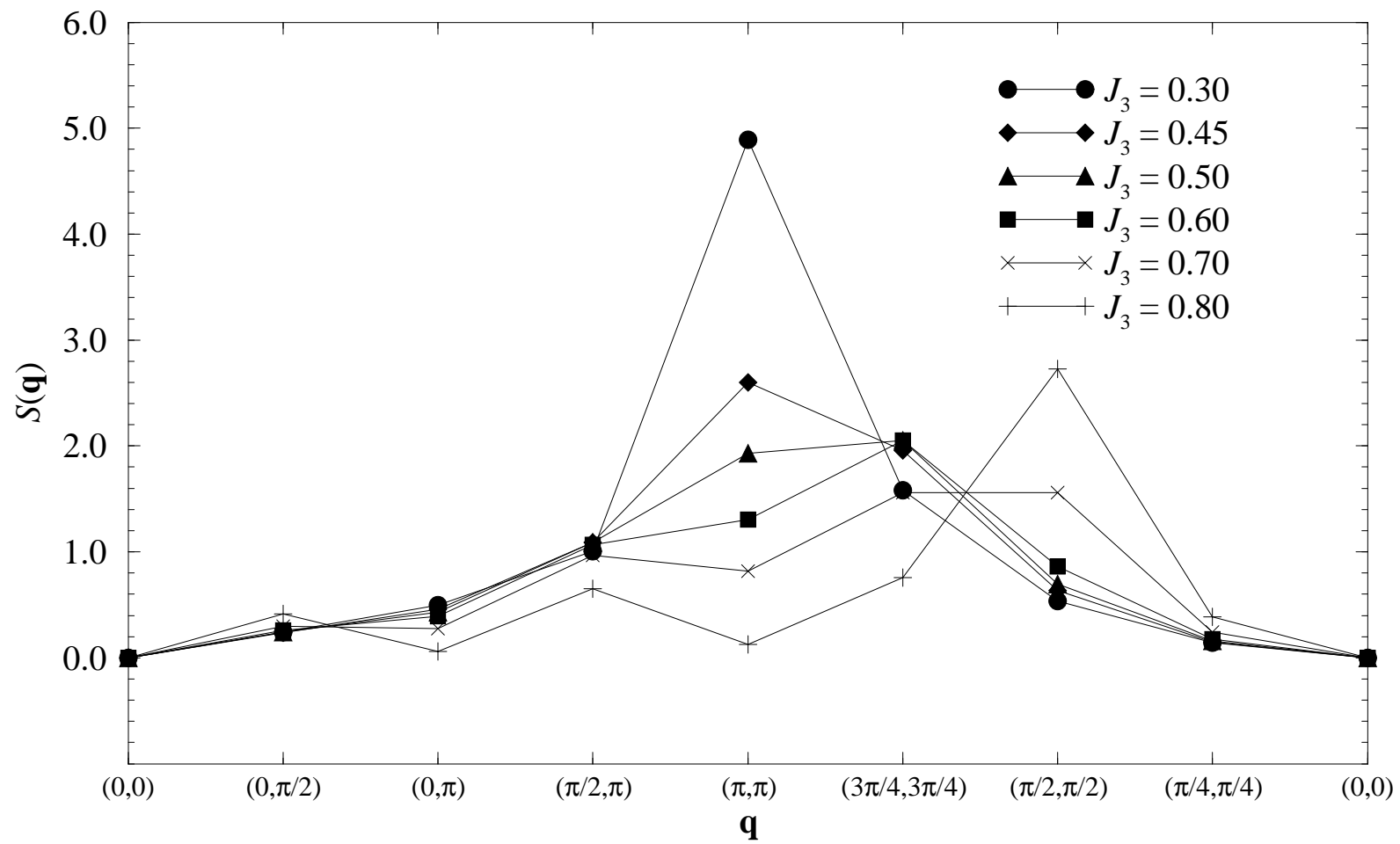
TABLE I. Dimer-dimer correlation functions for all inequivalent dimer pairs in the 32-site system at $J_3 = 0.7$. The reference pair is (19, 23). See Fig. 5 for the numbering of the sites.

(k,l)	$C_{(19,23)(k,l)}$	(k,l)	$C_{(19,23)(k,l)}$
(1,5)	0.055075	(18,22)	-0.054987
(1,29)	0.003783	(19,22)	-0.019733
(2,29)	0.051208	(21,25)	0.003865
(5,10)	-0.051912	(21,26)	-0.045224
(10,14)	0.067346	(22,26)	0.009617
(13,18)	0.051260	(22,27)	0.104930
(14,19)	-0.071722	(25,29)	-0.042596
(17,21)	0.050038	(26,29)	0.003208
(18,21)	0.002528	(26,30)	0.067526

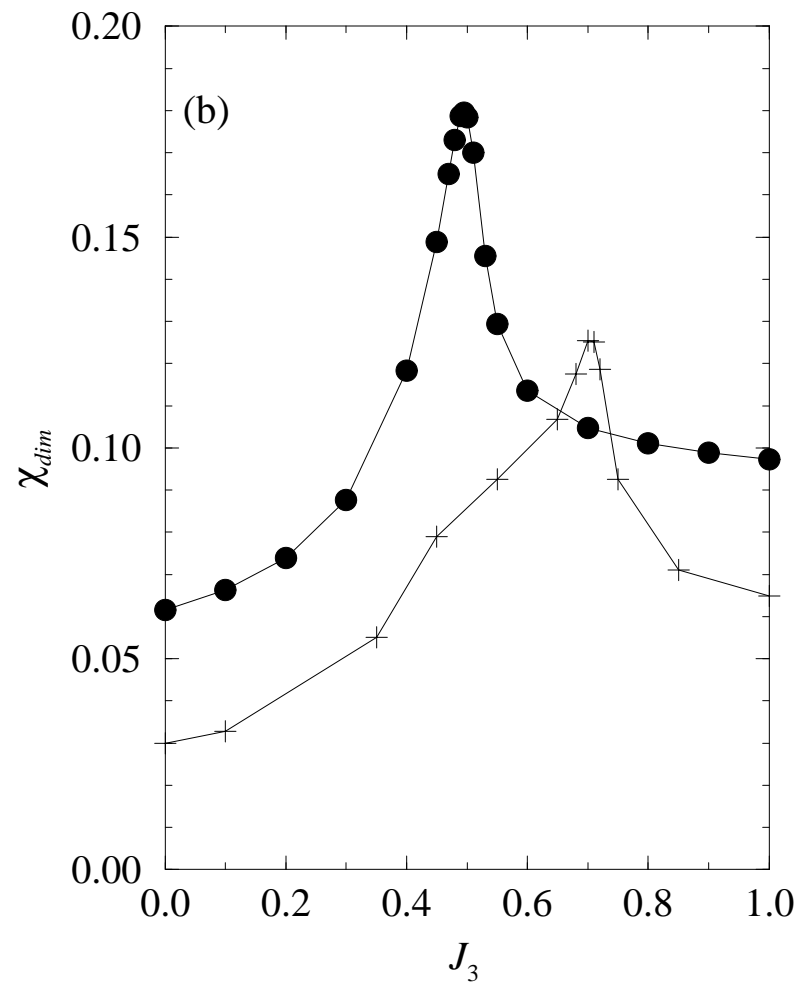
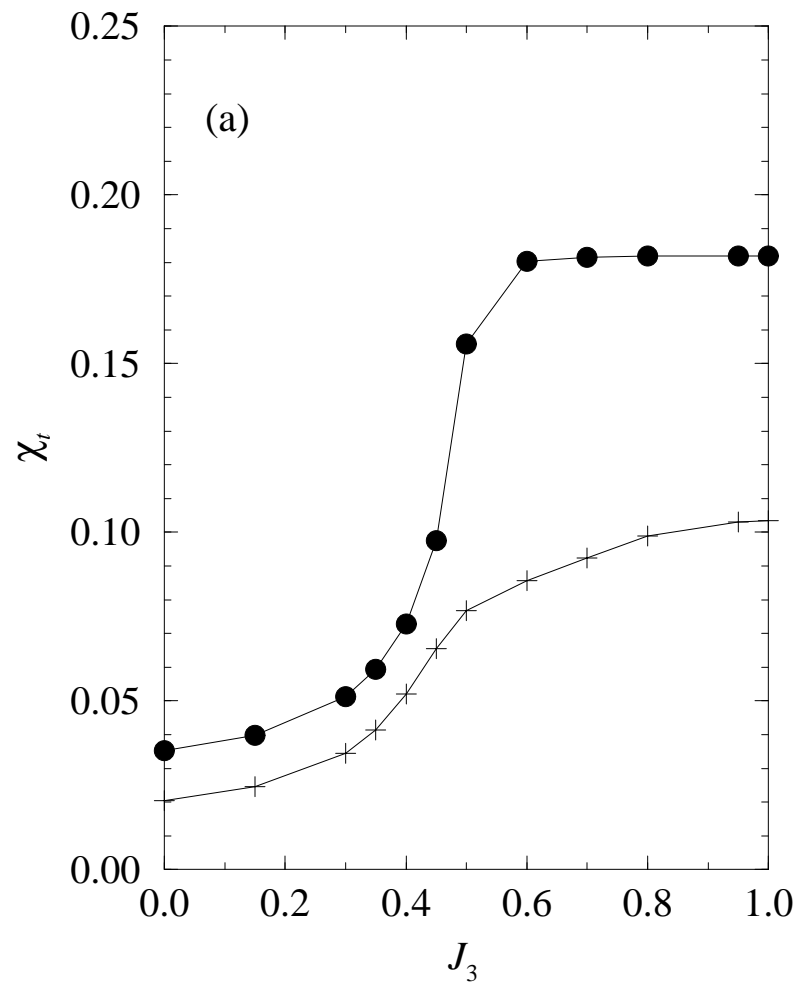
Leung and Lam Fig. 1



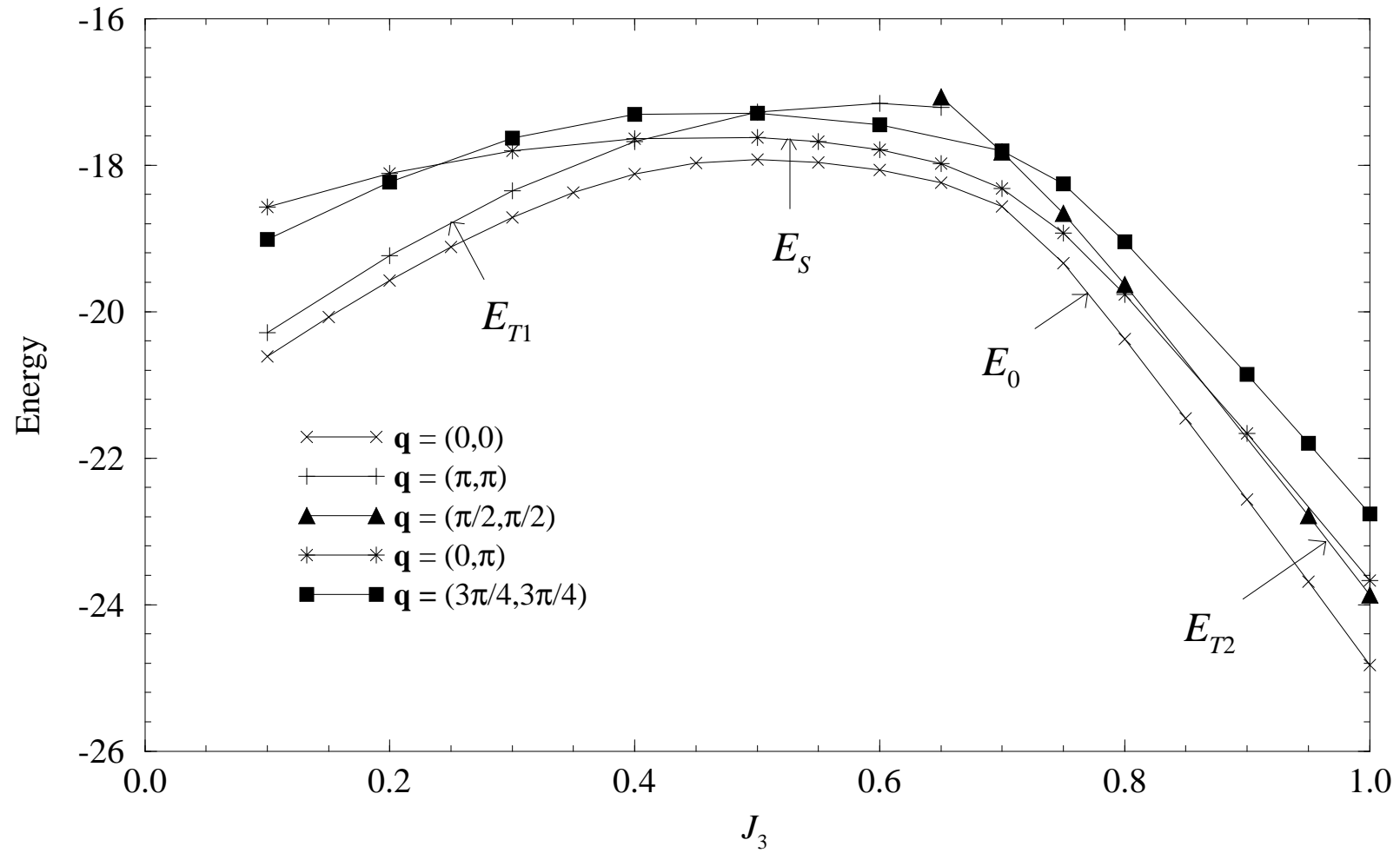
Leung and Lam Fig. 2



Leung and Lam Fig. 3



Leung and Lam Fig. 4



Leung and Lam Fig. 5

